

## 15. DATA REPORT: SULFIDE TEXTURES IN THE ACTIVE TAG MASSIVE SULFIDE DEPOSIT, 26°N, MID-ATLANTIC RIDGE<sup>1</sup>

D. Brown<sup>2</sup> and K.R. McClay<sup>3</sup>

### ABSTRACT

Ocean Drilling Program Leg 158 recovery from the active Trans-Atlantic Geotraverse (TAG) hydrothermal mound provided an excellent opportunity to study textures developed in an actively forming seafloor-hosted massive sulfide deposit. The TAG mound has a crude lithostratigraphy of approximately vertically stacked breccias that, at the base, consist of silicified and chloritized wall rock of the stockwork zone; at intermediate levels, they consist of sulfide-silica breccia clasts in an anhydrite matrix; and in the upper part they consist of massive sulfide breccias. Colloform pyrite-marcasite-sphalerite structures are the dominant sulfide textures developed in the upper part of the mound. At intermediate depths, sulfide textures are dominated by pyrite and chalcopyrite replacement of wall rock along anhydrite veins and by the recrystallization of sulfide grains. At depth, the deposit contains predominantly disseminated pyrite in a silicified wall-rock matrix, and sulfide veins cut the wall rock and altered basalt clasts. These textures and their distribution within the TAG deposit are remarkably similar to those described for the Cyprus ophiolite-hosted massive sulfide deposits.

### INTRODUCTION

Textural and paragenetic studies of massive sulfide deposits have generally been conducted on ancient, land-based deposits in which primary micro- and mesoscopic textures usually have been modified subsequent to formation of the deposit by processes such as deformation, metamorphism, or supergene alteration (e.g., McClay and Ellis, 1983; McClay, 1991; Gilligan and Marshall, 1987; Craig and Vokes, 1993). Consequently, important information on the primary development of massive sulfide deposits is either difficult to assess or missing. Ocean Drilling Program (ODP) Leg 158 recovery from the active TAG massive sulfide deposit at 26°N on the Mid-Atlantic Ridge provides a unique opportunity to study sulfide textures and paragenesis from the internal parts of what can be considered a modern-day analog, in terms of both internal structure and size, of ophiolite-hosted massive sulfide deposits such as those found in Cyprus and Bett's Cove, Newfoundland (e.g., Herzig and Hannington, 1995). Because little is known about the internal nature of actively forming massive sulfide deposits (with the exception of the Middle Valley deposit; Mottl, Davis, Fisher, Slack, 1994), previous studies have been largely confined to seafloor-surface samples obtained by dredging and submersible (e.g., Thompson et al., 1985; Rona et al., 1993; Fouquet et al., 1993; Graham et al., 1988), studies of textures in the TAG deposit provide important new information on how seafloor-hosted massive sulfide deposits form and evolve.

The internal structure of the TAG massive sulfide deposit consists of a complex association of sulfide-anhydrite-silica breccias, wall-rock breccias, and altered wall rock of the stockwork zone (Humphris, Herzig, Miller et al., 1996; Humphris et al., 1995). The TAG mound has a crude lithostratigraphy consisting of approximately vertically stacked breccias (Fig. 1) that, at the base, consists of silicified and chloritized wall rock of the stockwork zone. At intermediate levels, it consists of sulfide-silica breccia clasts in an anhydrite matrix, and, in the upper part, of massive sulfide breccias. Humphris, Herzig, Miller, et al. (1996) and Humphris et al. (1995) suggested

that the lithostratigraphic sequence may have formed as a result of multiple episodes of hydrothermal activity, faulting, and possibly collapse of the mound during inactive periods and noted that the deposit appears to grow as an in situ breccia pile. This paper presents textural data from pyrite, marcasite, sphalerite, and chalcopyrite, the dominant sulfide phases in the TAG deposit, from near-surface samples to those from a depth of 120 meters below seafloor (mbsf).

### SAMPLE PREPARATION

Samples were prepared as polished thin sections for transmitted-light microscopy and as polished blocks for reflected-light microscopy. Selected polished blocks were etched in warm 25% HNO<sub>3</sub> to study growth textures (e.g., grain boundaries and overgrowths), different mineral phases, and deformation textures (dissolution, brecciation, and recrystallization). The etching process is a simple and non-destructive technique in which the sample is immersed in warm etchant, with the process often repeated several times, until the desired degree of etching is achieved.

### TEXTURES

The uppermost part of the TAG deposit (from 0 to ~15 mbsf) consists predominantly of massive, commonly porous and brecciated pyrite. Colloform pyrite with very well-developed, micrometer-scale growth banding is by far the most common feature in this part of the deposit (Pl. 1, Fig. 1). Individual and composite colloform pyrite structures are cemented by fine-grained, typically cubic pyrite with micrometer-scale growth banding (Pl. 1, Fig. 2). The colloform banding is usually truncated against the cement, suggesting dissolution and precipitation processes have been active (Pl. 1, Fig. 3). Rarely, the banding is partly recrystallized into very fine grained, equant to anhedral, pyrite grains. These colloform structures are typically cored by an assemblage of crystalline pyrite, chalcopyrite, and sphalerite, indicative of mineral precipitation within a fluid conduit. Locally, these phases form a roughly equant structure, with a pyrite core, rimmed by chalcopyrite, and an outer rim of sphalerite (Pl. 1, Fig. 4), suggestive of a completely blocked conduit. In one location, fractures in pyrite are infilled with sphalerite and chalcopyrite (Pl. 1, Fig. 5). Equant to euhedral pyrite overgrowths, locally with 120° di-

<sup>1</sup>Herzig, P.M., Humphris, S.E., Miller, D.J., and Zierenberg, R.A. (Eds.), 1998. *Proc. ODP, Sci. Results*, 158: College Station, TX (Ocean Drilling Program).

<sup>2</sup>Instituto de Ciencias de la Tierra "Jaume Almera," CSIC, Lluís Sole i Sabaris s/n, 08028 Barcelona, Spain. dbrown@ija.csic.es

<sup>3</sup>Department of Geology, Royal Holloway, University of London, Egham, Surrey TW20 OEX, United Kingdom.

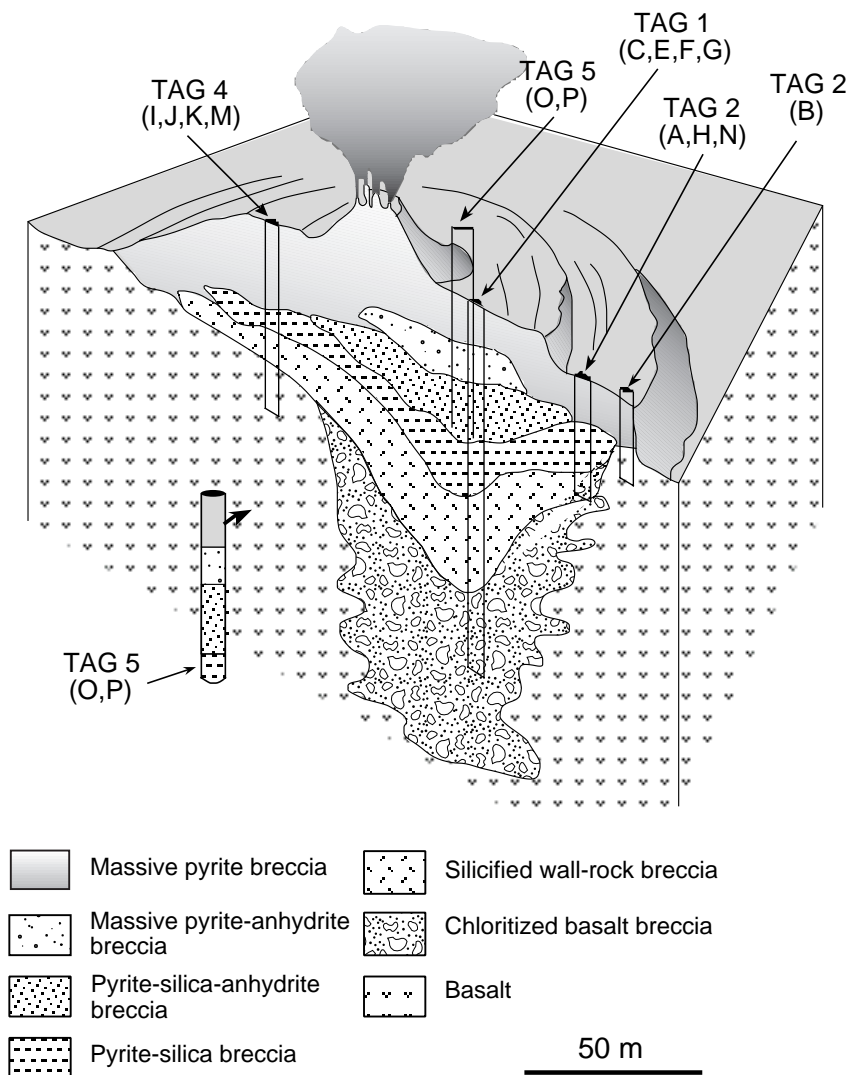


Figure 1. Sketch of the TAG mound showing the distribution of the various lithofacies and the location of the Leg 158 boreholes (after Humphris, Herzig, Miller et al., 1996; Humphris et al., 1995).

hedral angles, on colloform cores are common (Pl. 1, Fig. 3). Laminated pyrite with a euhedral, cubic morphology (Pl. 1, Fig. 6) is less common in the upper part of the deposit.

The majority of marcasite in the TAG deposit occurs within the upper 20 m (Humphris, Herzig, Miller et al., 1996). Marcasite generally occurs as colloform growth structures with numerous micrometer-scale growth laminae (Pl. 2, Fig. 1), commonly interbanded with colloform pyrite and sphalerite. Recrystallization of marcasite grains is widespread (Pl. 2, Fig. 2). Replacement of marcasite by anhedral, fine-grained pyrite is also widespread (Pl. 2, Fig. 1).

Like marcasite, the majority of sphalerite in the TAG deposit is found within the upper 20 m. By far the most common sphalerite texture is growth-banding of subhedral to euhedral grains, usually replacing both colloform and coarsely crystalline pyrite (Pl. 2, Fig. 3). True colloform sphalerite is rare, and it is typically interbanded with, and commonly replacing, colloform pyrite (Pl. 2, Fig. 4), or euhedral pyrite. Colloform sphalerite is intimately associated with growth-banded, subhedral to euhedral sphalerite grains, suggesting recrystallization of the colloform structures.

Chalcopyrite occurs throughout the deposit. The usual occurrence of chalcopyrite, at all depths in the deposit, is amorphous grain as-

semblages in selvages associated with anhydrite veining (see below). In the upper part of the deposit, chalcopyrite also forms the cores of, or replaces, colloform structures (see Pl. 1, Fig. 4).

At intermediate depths, between approximately 20 and 45 mbsf, the deposit consists of complex pyrite-anhydrite and pyrite-silica-anhydrite breccias. Sulfide growth in this part of the deposit appears to have been dominated by selva-related replacement associated with anhydrite veining. Selvages have a common sulfide mineralogy of chalcopyrite and pyrite, with lesser marcasite and minor sphalerite. A selva generally consists of chalcopyrite immediately adjacent to the vein anhydrite, followed by pyrite abutting the wall rock (Pl. 3, Fig. 1).

Textural relationships in these selvages indicate a complex chalcopyrite-pyrite paragenesis. Facing the vein, pyrite has moderately to well-developed growth banding extending roughly parallel to the vein wall (Pl. 3, Fig. 1). Chalcopyrite and marcasite are locally intergrown with the pyrite. Within, and facing the wall rock, pyrite grains are subhedral to euhedral, usually with multistage growth textures and widespread evidence of dissolution and precipitation (Pl. 3, Fig. 2). Recrystallization of pyrite is also widespread, and it is common that the new grain boundaries overgrow the multistage growth zon-

ing, partially or wholly overprinting it (Pl. 3, Fig. 3; locally, several new grain boundaries appear to be active simultaneously). An earlier generation of pyrite grains forms mottled inclusions within the new grains. Chalcopyrite also occurs as inclusions in pyrite, and rare pyrite veinlets cut the chalcopyrite, suggesting several phases of sulfide deposition and growth. Triangular to blocky chalcopyrite grains in the silicate wall rock suggest that it has pseudomorphically replaced a euhedral pyrite grain (Pl. 3, Fig. 4).

At intermediate depths in the deposit, marcasite generally occurs as growth-banded laminae that have been partially to extensively altered to pyrite (Pl. 3, Fig. 5). Sphalerite occurs as subhedral to anhedral, growth-banded grain aggregates, typically overgrowing pyrite (Pl. 3, Fig. 6).

In the deeper parts of the deposit (from approximately 45 to 120 mbsf), sulfide textures consist predominantly of subhedral to euhedral pyrite disseminated throughout silicified wall rock (Pl. 4, Fig. 1). These pyrite grains typically contain abundant quartz inclusions, and the bulging pyrite boundaries show clear evidence of replacement of quartz (Pl. 4, Fig. 2). Pyrite is also found in pyrite veinlets cutting the silicified wall rock (Pl. 4, Fig. 3) and altered basalt (Pl. 4, Fig. 4), where the silica has usually recrystallized along the veinlet margin to form quartz. In the upper part of this interval, pyrite and chalcopyrite selvages are also associated with silica veins in the silicified wall rock.

## DISCUSSION

The clear vertical distribution of sulfide textures in the TAG mound broadly represents different mechanisms of sulfide deposition and growth and evolution of the deposit at different levels. Colloform pyrite-marcasite-sphalerite structures in the upper part of the deposit most likely represent fluid conduits (c.f. Tivey et al., 1995), cemented by later subhedral to euhedral pyrite, suggesting that the main sulfide-forming mechanism in this part of the mound is by precipitation in areas of focused fluid flow. However, the cement infilling the areas between the colloform fluid conduits (Pl. 1, Fig. 2) further suggests that diffuse fluid flow played an active role in sulfide formation in the upper part of the deposit. The occurrence of fractures with an infill of sulfide (Pl. 1, Fig. 5) indicates overpressuring and hydraulic fracturing may have taken place, perhaps as conduits became blocked by sulfide precipitation (Pl. 1, Fig. 4). Selvages associated with anhydrite veining were also an important sulfide-forming (particularly chalcopyrite) mechanism in the upper part of the deposit.

At intermediate depths, sulfide selvages associated with anhydrite veining become more important as areas of sulfide deposition. The common mineralization sequence within selvages (Pl. 3, Fig. 1) may represent the evolution of the ore-forming fluid as it cools and/or mixes, with the higher temperature fluid represented by pyrite and progressively lower temperatures by chalcopyrite and, finally, vein anhydrite precipitating from entrained seawater. Alternation and intergrowth of the sulfide phases in the selvages, together with widespread evidence for replacement, recrystallization, and phase transformations (i.e., marcasite to pyrite), possibly indicate changes in fluid composition, temperature, and pH, and fluctuations in the activity and fugacity of  $S_2$  and  $O_2$  (e.g., Hemley et al., 1992; Marchig et al., 1988; Hannington et al., 1995; Tivey et al., 1995). Sulfide veining is more common in the deeper parts of the deposit, but the textural relationships observed between pyrite and quartz indicate that fluctuations in the activity and fugacity of  $S_2$  and  $O_2$  also play an important role in sulfide mineralization in the stockwork zone.

The sulfide textures and vertical zoning developed in the TAG deposit are remarkably similar to those found in Cyprus deposits (Con-

stantinou, 1976, 1980). The development of similar textures in the TAG deposit clearly point to the possibility of a primary origin for features such as colloform pyrite and the cementing euhedral pyrite, which in the Cyprus deposits are thought to be secondary in nature (Constantinou, 1976, 1980).

## CONCLUSIONS

The widespread occurrence of vein systems, dissolution, recrystallization, replacement, and phase changes in the TAG deposit point toward a dynamic, changing hydrothermal system in which fluid flux plays an important role in the mineralogical and textural evolution of the deposit. These textures also indicate that the sulfide phases throughout the deposit are undergoing frequent, if not constant, textural, and most likely chemical, modification, and suggest that the evolution of a seafloor massive sulfide deposit involves a long and complex history of growth and internal replacement. Significantly, many of the textures found in the TAG deposit are similar to those described in on-land ophiolite-hosted massive sulfide deposits, suggesting that features previously thought to be secondary are, in fact, primary.

## ACKNOWLEDGMENTS

Brown is funded by a CICYT post-doctoral fellowship. Financial help from the Department of Geology, Royal Holloway, University of London, for sample preparation is also gratefully acknowledged. Reviews by W. Goodfellow and S. Humphris improved the manuscript.

## REFERENCES

- Constantinou, G., 1976. Genesis of the conglomerate structure, porosity and colomorph textures of the massive sulphide ores of Cyprus. *In* Strong, D.F. (Ed.), *Metallogeny and Plate Tectonics*. Spec. Pap. Geol. Assoc. Can., 14:187-210.
- , 1980. Metallogenesis associated with the Troodos ophiolite. *In* Panayiotou, A. (Ed.), *Ophiolites*. Proc. Int. Ophiolite Symp. Cyprus, Cyprus Geol. Surv. Dep., 663-674.
- Craig, J.R., and Vokes, F.M., 1993. The metamorphism of pyrite and pyritic ores: an overview. *Mineral. Mag.*, 57:3-18.
- Fouquet, Y., Wafik, A., Cambon, P., Mevel, C., Meyer, G., and Gente, P., 1993. Tectonic setting and mineralogical and geochemical zonation in the Snakepit sulphide deposit (Mid-Atlantic Ridge at 23°N). *Econ. Geol.*, 88:2018-2036.
- Gilligan, L.B., and Marshall, B., 1987. Textural evidence for remobilisation in metamorphic environments, I. Mechanical and chemical (re) mobilisation of metaliferous mineralization. *Oreg. Geol. Rev.*, 2:205-230.
- Graham, U.M., Bluth, G.J., and Ohmoto, H., 1988. Sulfide-sulfate chimneys on the East Pacific Rise, 11° and 13° N latitudes. Part 1: mineralogy and paragenesis. *In* Barret, T.J., and Jambor, J.L. (Eds.), *Seafloor Hydrothermal Mineralization*. Can. Mineral., 26:487-504.
- Hannington, M.D., Jonasson, I.R., Herzig, P.M., and Petersen, S., 1995. Physical, chemical processes of seafloor mineralization at mid-ocean ridges. *In* Humphris, S.E., et al. (Eds.), *Seafloor Hydrothermal Systems: Physical, Chemical, Biological and Geological Interactions*. Am. Geophys. Union Monogr., 91:115-157.
- Hemley, J.J., Cygan, G.L., Fein, J.B., Robinson, G.R., and D'Angelo, W.M., 1992. Hydrothermal ore-forming processes in the light of studies in rock-buffered systems, I. Iron-copper-zinc-lead sulfide solubility relations. *Econ. Geol.*, 87:1-22.
- Herzig, P.M., and Hannington, M.D., 1995. Polymetallic massive sulfides at the modern seafloor—a review. *Ore Geol. Rev.*, 10:95-115.

- Humphris, S.E., Herzig, P.M., Miller, D.J., Alt, J.C., Becker, K., Brown, D., Brüggmann, G., Chiba, H., Fouquet, Y., Gemmel, J.B., Guerin, G., Hannington, M.D., Holm, N.G., Honnorez, J.J., Itturino, G.J., Knott, R., Ludwig, R., Nakamura, K., Petersen, S., Reysenbach, A.-L., Rona, P.A., Smith, S., Sturz, A.A., Tivey, M.K., and Zhao, X., 1995. The internal structure of an active sea-floor massive sulphide deposit. *Nature*, 377:713–716.
- Humphris, S.E., Herzig, P.M., Miller, D.J., et al., 1996. *Proc. ODP, Init. Repts.*, 158: College Station, TX (Ocean Drilling Program).
- Marchig, V., Rosch, H., Lalou, C., Bricet, E., and Oudin, E., 1988. Mineralogical zonation and radiochronological relations in a large sulfide chimney from the East Pacific Rise at 18°25' S. *Can. Mineral.*, 26:541–554.
- McClay, K.R., 1991. Deformation of stratiform Zn-Pb (-barite) deposits in the northern Canadian Cordillera. *Oreg. Geol. Rev.*, 6:435–462.
- McClay, K.R., and Ellis, P.G., 1983. Deformation and recrystallisation of pyrite. *Mineral. Mag.*, 47:527–538.
- Mottl, M.J., Davis, E.E., Fisher, A.T., and Slack, J.F. (Eds.), 1994. *Proc. ODP, Sci. Results*, 139: College Station, TX (Ocean Drilling Program).
- Rona, P.A., Hannington, M.D., Raman, C.V., Thompson, G., Tivey, M.K., Humphris, S.E., Lalou, C., and Petersen, S., 1993. Active and relict sea-floor hydrothermal mineralization at the TAG hydrothermal field, Mid-Atlantic Ridge. *Econ. Geol.*, 88:1987–2013.
- Thompson, G., Mottl, M.J., and Rona, P.A., 1985. Morphology, mineralogy and chemistry of the hydrothermal deposits from TAG area, 26°N, Mid-Atlantic Ridge. *Chem. Geol.*, 49:243–257.
- Tivey, M.K., Humphris, S.E., Thompson, G., Hannington, M.D., and Rona, P.A., 1995. Deducing patterns of fluid flow and mixing within the TAG active hydrothermal mound using mineralogical and geochemical data. *J. Geophys. Res.*, 100:12,527–12,555.

**Date of initial receipt: 23 May 1996**

**Date of acceptance: 2 May 1997**

**Ms 158SR-224**

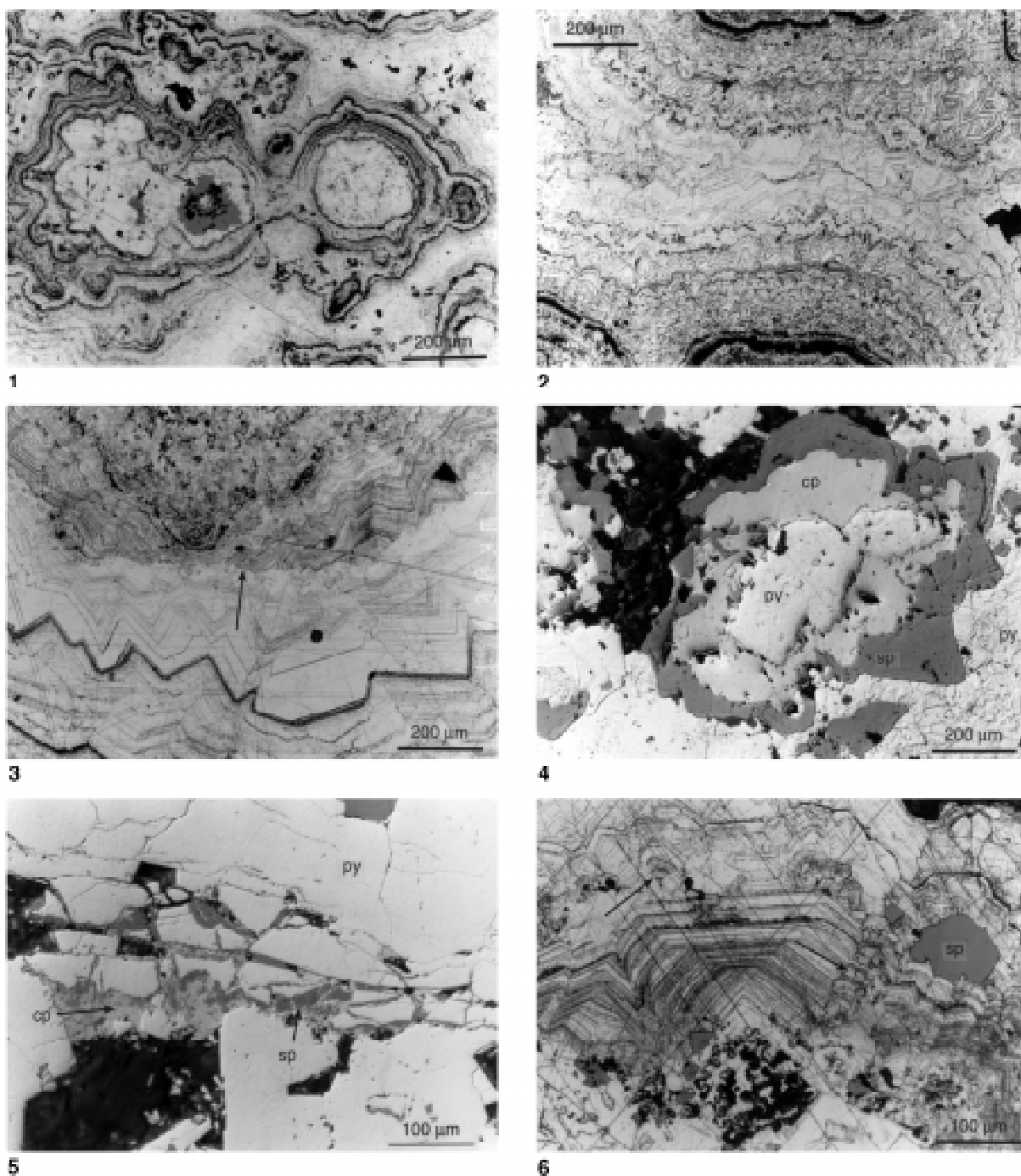


Plate 1. **1.** Colloform pyrite showing micrometer-scale growth banding. The central part of the colloform structures is infilled by pyrite, chalcopyrite, and sphalerite (sp). Sample 158-957I-1N-1, 42–46 cm. Etched in 25%  $\text{HNO}_3$  Normarski interference contrast. **2.** Colloform structures are cemented by euhedral pyrite with numerous growth bands. Sample 158-957E-10R-1, 9–10 cm. Etched in 25%  $\text{HNO}_3$  Normarski interference contrast. **3.** Colloform structures are truncated by the cement, indicating that dissolution (arrow) and precipitation have occurred. Sample 158-957I-1N-1, 53–56 cm. Etched in 25%  $\text{HNO}_3$  Normarski interference contrast. **4.** Roughly equant texture with pyrite (py) in the center, surrounded by chalcopyrite (cp), and the whole rimmed by sphalerite (sp). Sample 158-957M-4R-1, 23–24 cm. Etched in 25%  $\text{HNO}_3$  Normarski interference contrast. **5.** Fractured pyrite (py) with the fracture infilled by chalcopyrite (cp) and sphalerite (sp). Sample 158-957M-4R-1, 2–4 cm. **6.** Growth-banded pyrite with a euhedral morphology. There are several phases of pyrite growth present, represented by various morphologies. Note that there is local recrystallization of pyrite (arrows) and late sphalerite (sp) also replaces pyrite. Sample 158-957I-1N-1, 18–23 cm. Etched in 25%  $\text{HNO}_3$  Normarski interference contrast.

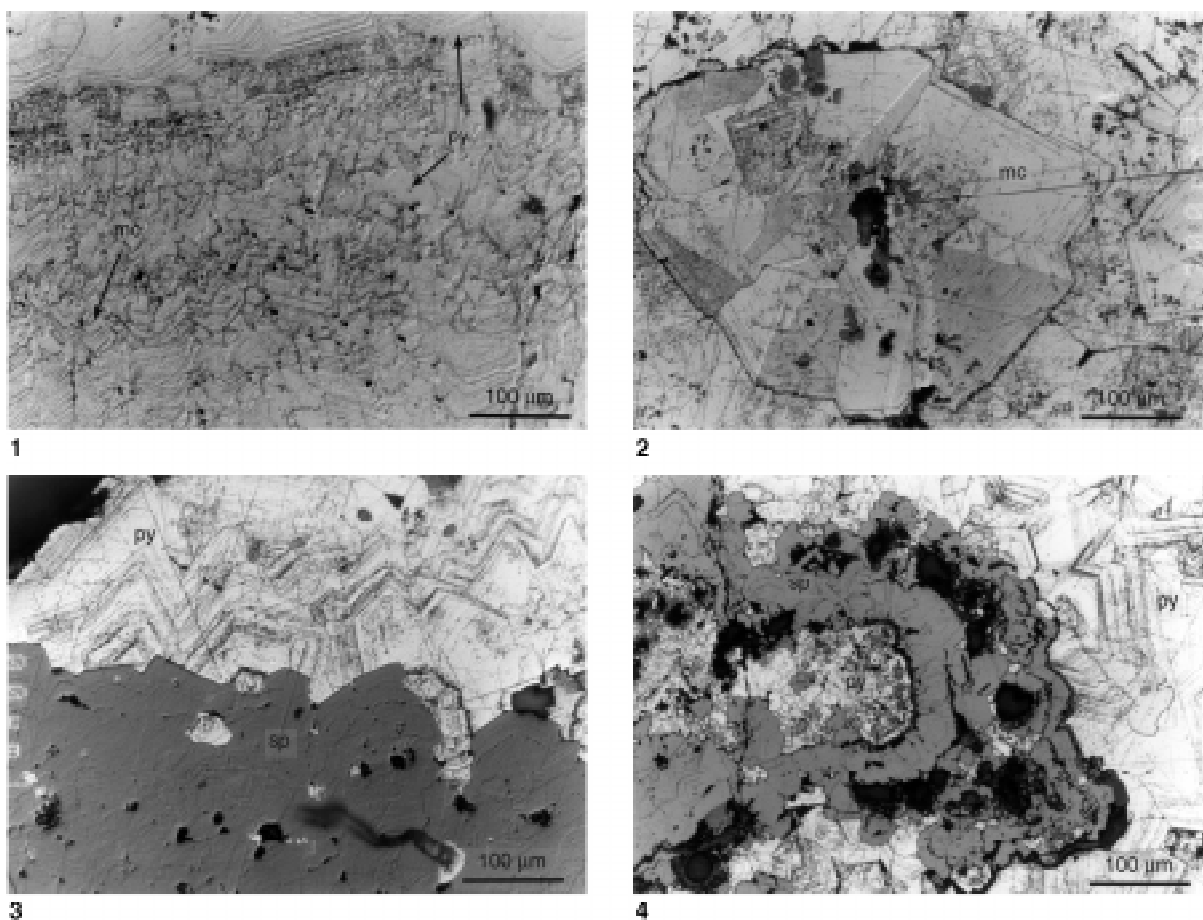
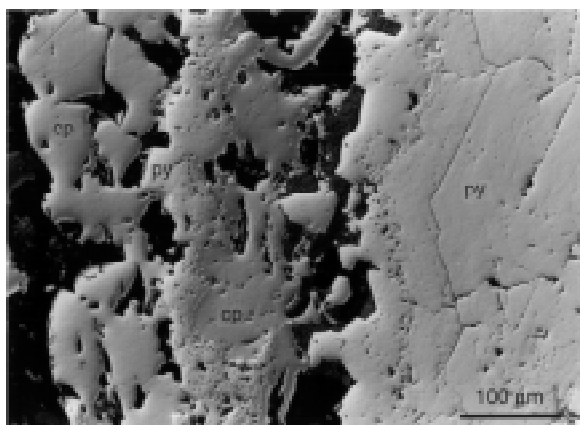
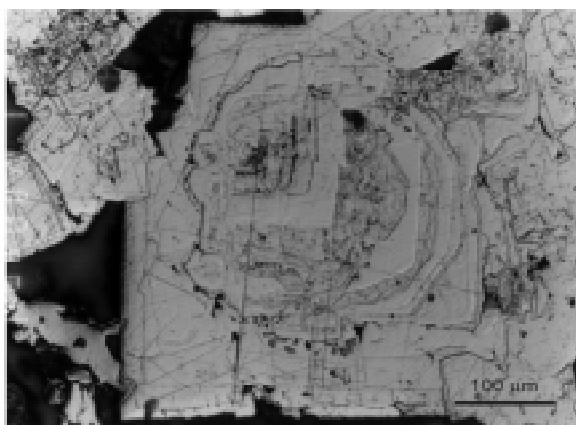


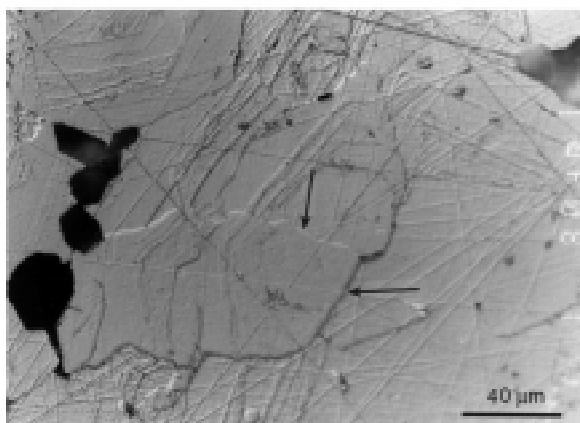
Plate 2. **1.** Growth-banded marcasite that is altering to anhedral pyrite (py). Sample 158-957M-4R-7, 2–4 cm. Etched in 25% HNO<sub>3</sub> Normarski interference contrast. **2.** Subhedral grain of marcasite (mc) undergoing recrystallization. 158-957C-10N-1, 38–42 cm. Etched in 25% HNO<sub>3</sub> Normarski interference contrast. **3.** Sphalerite (sp) replacing euhedral, growth-banded pyrite (py). Sample 158-957M-3R-1, 27–28 cm. Etched in 25% HNO<sub>3</sub> Normarski interference contrast. **4.** Colloform sphalerite (sp) replacing colloform and euhedral pyrite (py). Note that in the bottom left of the photograph, sphalerite has recrystallized to form euhedral grains. Sample 158-957M-3R-1, 53–55 cm. Etched in 25% HNO<sub>3</sub> Normarski interference contrast.



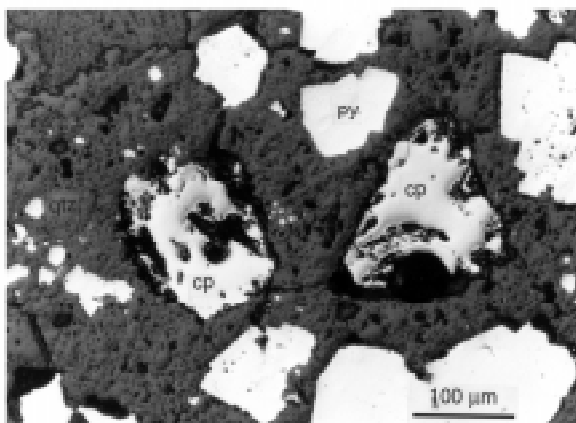
1



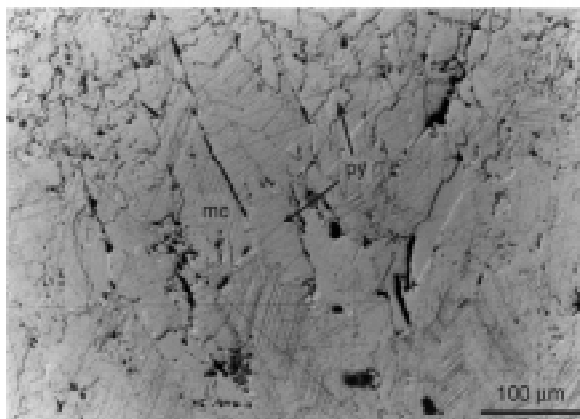
2



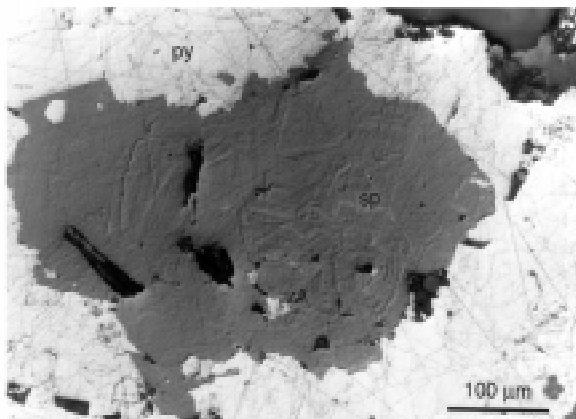
3



4



5



6

Plate 3. 1. Chalcopyrite (cp) and pyrite (py) selvage along an anhydrite vein. Note the well-developed banding in the pyrite, parallel to the vein wall. Sample 158-957C-7N-2, 81–82 cm. 2. Growth-banded, euhedral pyrite displaying multiple stages of dissolution and overgrowth. Sample 158-957P-6R-1, 18–20 cm. Etched in 25% HNO<sub>3</sub> Normarski interference contrast. 3. Recrystallizing pyrite with two active grain boundaries growing (arrows). Sample 158-957C-11N-1, 60–63 cm. Etched in 25% HNO<sub>3</sub> Normarski interference contrast. 4. Triangular and blocky chalcopyrite (cp) grain that has pseudomorphically replaced a euhedral pyrite (py) grain. Sample 158-957N-1W-16, 45–50 cm. 5. Finely banded marcasite (mc) recrystallizing to pyrite (py). Sample 158-957M-8R-1, 8–12 cm. Etched in 25% HNO<sub>3</sub> Normarski interference contrast. 6. Growth-banded sphalerite (sp) replacing pyrite (py). Sample 158-957M-8R-1, 8–12 cm. Etched in 25% HNO<sub>3</sub> Normarski interference contrast.

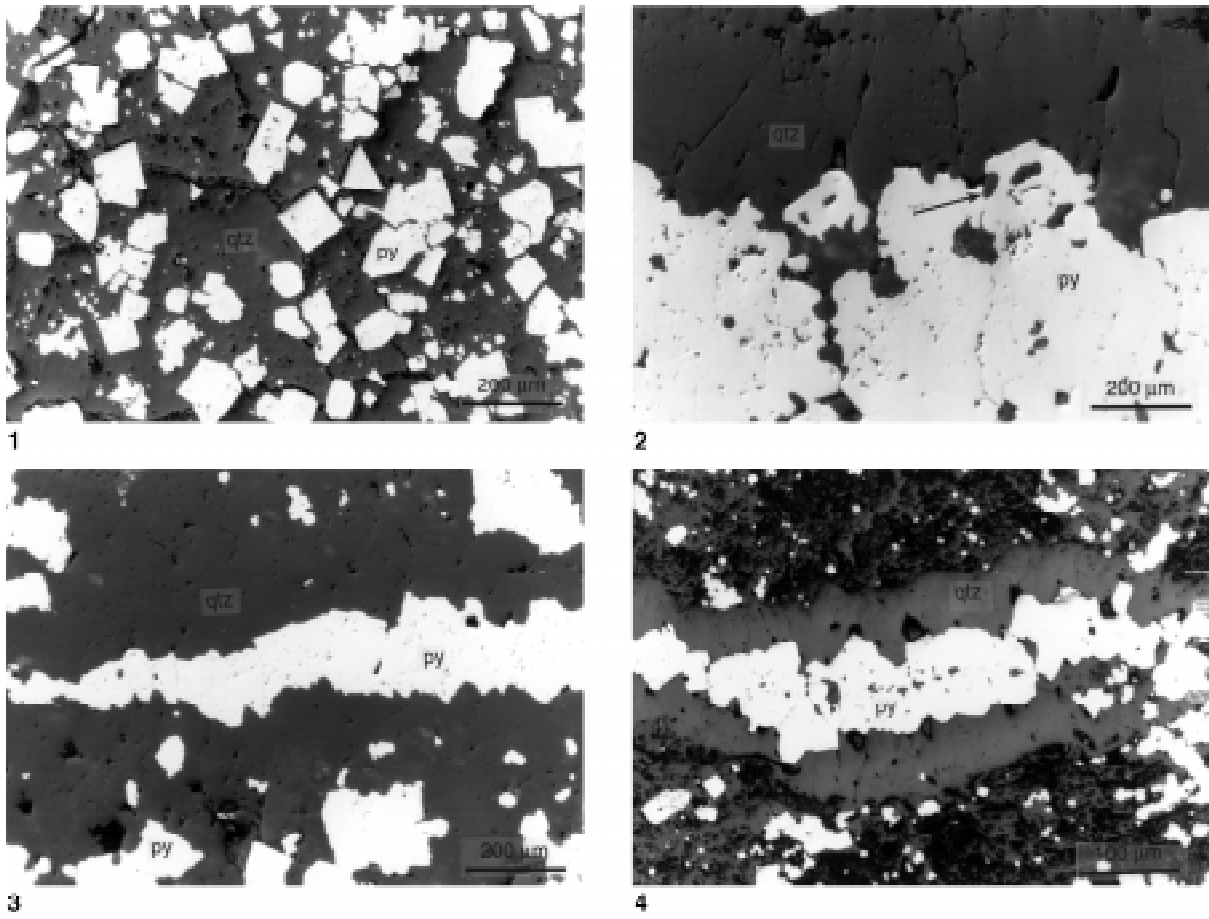


Plate 4. **1.** Disseminated, euhedral pyrite (py) in a silica (qtz) matrix. Sample 158-957N-1W-1, 53–58 cm. **2.** Pyrite replacing quartz (arrow). Sample 158-957C-16N-1, 38–42 cm. **3.** Pyrite (py) vein cutting silicified wall rock. Sample 158-957P-12R-4, 80–82 cm. **4.** Pyrite (py) vein cutting an altered basalt clast. Note that the silica (qtz) has recrystallized along the margin of the vein. Sample 158-957E-14R-1, 48–52 cm.